land

MDPI

Article

Water Retention and Availability in an Ultisol Under an Integrated Crop–Livestock–Forest System in the Matopiba Region, Brazil

Maria Laiane do Nascimento Silva [1,*], Luiz Fernando Carvalho Leite [1], Flávio Pereira de Oliveira [2], Flavio Favaro Blanco [1], Henrique Antunes de Souza [1], Ivana Tito Sousa [2], Thais Santiago de Sousa [1], Edvaldo Sagrilo [1], Daniel Silva Veras [3], Reurysson Chagas de Sousa Morais [3] and José Oscar Lustrosa Oliveira Junior [1]

[1] Brazilian Agricultural Research Corporation, EMBRAPA Mid-North, Teresina 64008-780, PI, Brazil; luiz.f.leite@embrapa.br (L.F.C.L.); flavio.blanco@embrapa.br (F.F.B.); henrique.souza@embrapa.br (H.A.d.S.); santthaiis@gmail.com (T.S.d.S.); edvaldo.sagrilo@embrapa.br (E.S.); jose.oscar@embrapa.br (J.O.L.O.J.)
[2] Department of Soils and Rural Engineering, Federal University of Paraíba—UFPB, Areia 58397-000, PB, Brazil; flavio.oliveira@academico.ufpb.br (F.P.d.O.); ivana.tito@academico.ufpb.br (I.T.S.)
[3] Federal Institute of Education of Piauí-IFPI, Teresina 64008-780, PI, Brazil; danielveras@ifpi.edu.br (D.S.V.)
* Correspondence: mlnslaiane@gmail.com

Abstract

Soil water retention and availability are influenced by intrinsic soil properties, management practices, and climate regimes. This study aimed to evaluate water retention and availability in an Ultisol under different integrated production systems in the Brazilian Cerrado. The systems analyzed included Crop–Livestock Integration (CLI), Livestock–Forest Integration (LFI), Crop–Forest Integration (CFI), no-tillage (NT) and native Cerrado vegetation (NV). Disturbed samples were collected for physical and chemical characterization, while undisturbed samples were used to determine water retention curves at depths of 0.00–0.10, 0.10–0.20, and 0.20–0.40 m. From these curves, water availability, pore-size distribution, differential log-pore-radius curves, most frequent pore radius, and relative hydraulic conductivity were estimated using the Mualem–van Genuchten model. Confidence intervals were used to evaluate differences between retention curves. The CLI system showed lower water content at saturation (14–30%) and field capacity (10–20%) compared to CFI, LFI, and NT. The NT system exhibited higher water availability across all layers (28, 48, and 46%, respectively) than CLI. Alterations in pore structure, likely due to the short integration period and monoculture history in CLI, resulted in lower water retention. Conversely, CFI, LFI, and NT showed higher retention and availability, attributed to higher organic matter content and more stable structural pores. Integrated production and no-tillage systems, especially when adopted long-term, enhance soil water retention and availability in the Brazilian Cerrado.

Keywords: soil physical–hydraulic properties; water retention curve; regenerative agriculture; Cerrado biome; climate change

Academic Editors: Jinglong Fan, Sameh Kotb Abd-Elmabod and Lei Wang

Received: 9 January 2026
Revised: 15 February 2026
Accepted: 19 February 2026
Published: 24 February 2026

1. Introduction

Brazilian agricultural production, particularly grain production, is highly dependent on rainfall [1]. However, deforestation and land-use change have disrupted fundamental processes of the hydrological cycle by altering the surface energy balance and soil hydrological functioning, leading to climatic irregularities at different spatial and temporal

scales [2–4]. These effects have become increasingly evident in recent decades, especially in areas undergoing intense agricultural expansion, such as the agricultural frontier in Brazil that encompasses parts of the states of Maranhão, Tocantins, Piauí, and Bahia, collectively known as Matopiba, where consistent signs of reduced precipitation and rising temperatures have already been reported [5,6]. In addition, soil degradation associated with land-use change and inadequate management reduces infiltration capacity, increases surface runoff, and decreases groundwater recharge, thereby exacerbating water insecurity for agricultural production [7–9].

In the Cerrado region of eastern Maranhão, within the context of agricultural expansion in Matopiba, typical dystrocohesive Yellow Argisols (Argissolos Amarelos Distrocoesos; Ultisols) predominate. These soils are sandy, structurally fragile, and highly susceptible to degradation when subjected to intensive land-use systems. This vulnerability arises primarily from the combined effects of low water retention capacity, low organic matter content, and the presence of cohesive horizons, which together accelerate degradation processes and reduce productive capacity [10].

Within this framework, integrated production systems—based on the synergistic combination of agricultural, livestock, and forest components—have been recognized as a sustainable technological innovation, promoting the restoration of degraded soils, increasing water availability to plants, and reducing the risk of yield losses [11–15]. The adoption of this approach, widely known as the Integrated Crop–Livestock–Forest (ICLF) system, is based on the temporal and spatial interaction among annual crops, pastures, and tree components and has yielded positive outcomes in other regions of Brazil [16–20]. This diversified agroecosystem promotes beneficial effects on the physical, chemical, and biological properties of the soil, contributing to soil health, ecological functionality, and the sustainability of agricultural systems [6,21–24]. Owing to these combined benefits, the ICLF system has been recognized as a regenerative agriculture practice—a systemic approach focused on restoring natural resources, strengthening biodiversity, and continuously improving soil quality [17,19,20].

From a physical–hydraulic perspective, ICLF systems are promoted as an alternative for increasing resilience to drought and water insecurity, as they enhance soil structure and water storage [19,25,26]. These systems increase infiltration and plant-available water capacity, thereby mitigating the effects of water stress, even during prolonged dry periods [22,27–29]. In the sandy and cohesive soils of the eastern Maranhão Cerrado, the adoption of such systems has been more effective in improving the soil physical–hydraulic quality than exclusive no-tillage systems, resulting in greater water retention and availability and often reaching values close to those observed under native vegetation [10]. This structural effect is further reinforced by the accumulation of organic matter derived from crop diversity, which improves soil porosity [10,30].

The soil water retention curve (SWRC) describes the relationship between matric potential and soil water content and is an essential soil property for the prediction of physical attributes, soil management, and hydrological modeling [31]. The shape of the retention curve reflects pore-size distribution, enables inferences about soil microstructure—such as the S index—and supports the derivation of hydraulic indicators, including field capacity, permanent wilting point, plant-available water capacity, air-filled porosity, and the least limiting water range [15,31]. These indicators integrate the relationships among water retention, aeration, and mechanical resistance, providing a functional assessment of soil physical quality. Furthermore, the water retention curve supports the modeling of water movement, infiltration, and water availability, with its parameters being used in hydrological model calibration, the development of pedotransfer functions, and the evaluation of the impacts of different management systems on soil structure and functioning [6,30,32].

Thus, the SWRC constitutes a central link among soil structure, hydrological dynamics, management practices, and soil resilience to climatic stress [33].

However, few studies in the Matopiba region—particularly in the eastern Maranhão Cerrado—have evaluated how integrated systems contribute to soil water retention and availability from a perspective that explicitly accounts for climate change and rainfall irregularity, which is fundamental for productive sustainability. Therefore, this study aimed to evaluate soil water retention and availability in an Ultisol under integrated production systems in the Matopiba region of the Brazilian Cerrado.

2. Materials and Methods

2.1. Study Area and Management Systems

The study was conducted at Barbosa Farm (2°50′ S, 42°29′ W; altitude 120 m), located in the municipality of Brejo, eastern Maranhão, Northeast Brazil. The farm comprises several productive activities, with emphasis on annual crops (950 ha) and beef cattle production (100 ha). Native vegetation corresponds to the Cerrado biome, with gently undulating to undulating relief. The climate is classified as Aw (Köppen–Geiger), indicating a tropical hot and humid climate, with mean annual temperature and precipitation of 27 °C and 1835 mm, respectively. The predominant soil is a typical dystrocohesive Yellow Argisol (Argissolo Amarelo distrocoeso típico [34]), equivalent to an Ultisol according to the Soil Taxonomy system [35].

Four management systems were evaluated—three integrated systems and one simplified monoculture system—in addition to an area under native vegetation: (1) Crop–Livestock Integration (CLI) under a soybean–Brachiaria intercropping system (*Brachiaria brizantha* cv. Marandu); (2) Livestock–Forest Integration (LFI); (3) Crop–Forest Integration (CFI); (4) no-tillage system (NT) under soybean (*Glycine max*); and (5) native Cerrado vegetation (NV) (Figure 1).

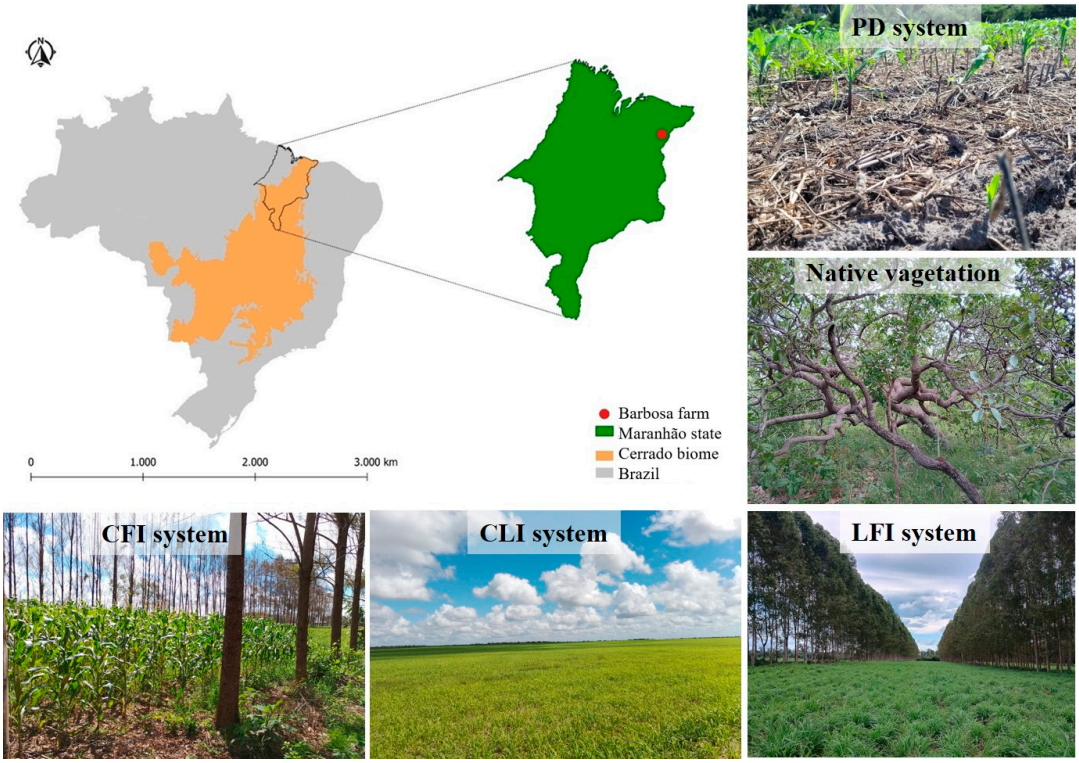

Figure 1. Location and land-use systems evaluated in the Maranhão state, Cerrado biome, Brazil.

The CLI area was cleared in 2003, with intensive soil disturbance (plowing and harrowing). Soybean cultivation began in 2004 and continued until 2021. At the end of 2021, the Crop–Livestock Integration system was implemented under a maize–Brachiaria intercropping system, with the introduction of cattle at a stocking rate of 0.7 animal units per hectare during the off-season. In 2024, soybean was cultivated under no-tillage management, and crop residues were incorporated into the soil after harvest.

The LFI area was cleared in 2004. In the following year, upland rice was cultivated and maintained until 2010. In 2011, Brachiaria was intercropped with maize, and cattle grazing was introduced after maize harvest. From 2021 onward, the Livestock–Forest Integration system was established using a consortium of eucalyptus (*Eucalyptus globulus*) and Mombaça grass (*Panicum maximum*), with a stocking rate of 0.7 animal units per hectare.

The CFI area was cleared up in 2004 and subsequently cultivated with upland rice. Between 2006 and 2010, soybean was grown under a monoculture system, and from 2011 onward, *Urochloa brizantha* cv. Marandu was intercropped with maize, with cattle grazing after maize harvest. Until 2017, successive soybean/millet cropping was practiced, followed by the establishment of eucalyptus tree rows in the same year. In February 2017, maize–forage intercropping was implemented between the eucalyptus rows. From 2018 to 2021, soybeans were cultivated between the eucalyptus rows, with soybean as the main crop and millet as the off-season cover crop. In 2023, peanuts (*Arachis hypogaea* L.) were cultivated between the eucalyptus rows.

The NT area was cleared in 2003 and initially managed under mechanized agriculture with conventional tillage, intensive soil disturbance, and the application of soil amendments and fertilizers. In the following year, soil conservation practices were adopted, including reduced tillage and soybean planting. In 2005, the no-tillage system was established and has been maintained to the present day under a soybean/millet succession system.

The NV area corresponds to native Cerrado vegetation, with sporadic fire occurrences during the dry season, which influence vegetation dynamics and local biodiversity.

2.2. Soil Sampling and Characterization

In each management system, disturbed soil samples were randomly collected, totaling five composite samples (each composed of three individual subsamples) at depths of 0.00–0.10, 0.10–0.20, and 0.20–0.40 m. These samples were used for chemical characterization, particle-size analysis, and quantification of soil organic carbon stocks (SOCS) (Tables 1 and 2).

Table 1. Chemical characterization (means + standard deviations) of a typical dystrocohesive Yellow Argisol (Ultisol) under different management systems in the Cerrado of Maranhão, Brazil (0.0–0.40 m).

Land Use *	pH	P	K^+	Na^+	Ca^{2+}	Mg^{2+}	Al^{3+}	SOM
	H_2O	$kg \cdot m^{-3}$	$mmolc \cdot kg^{-1}$					$g \cdot kg^{-1}$
	0.0–0.10 m							
CFI	5.7 ±0.18	0.028 ±0.007	0.48 ±0.161	0.102 ±0.058	13.9 ±2.54	5.9 ±2.11	0.7 ±0.5	29.9 ±8.8
CLI	6.4 ±0.28	0.070 ±0.023	0.91 ±0.24	0.099 ±0.023	9.5 ±1.63	5.0 ±0.79	0.0 ±0.1	26.0 ±8.8
LFI	6.3 ±0.39	0.009 ±0.004	3.17 ±1.12	0.186 ±0.068	20.6 ±4.45	7.3 ±1.87	0.3 ±0.5	43.5 ±6.0
NV	5.3 ±0.25	0.003 ±0.001	0.39 ±0.136	0.238 ±0.103	6.4 ±2.29	3.7 ±1.02	6.2 ±3.3	28.7 ±5.3
NT	5.4 ±0.22	0.029 ±0.009	0.49 ±0.102	0.019 ±0.011	6.9 ±2.5	3.1 ±0.68	3.3 ±3	29.6 ±4.25

Table 1. *Cont.*

Land Use *	pH	P	K^+	Na^+	Ca^{2+}	Mg^{2+}	Al^{3+}	SOM
	H_2O	kg · m^{-3}	mmolc · kg^{-1}					g · kg^{-1}
0.10–0.20 m								
CFI	5.5 ±0.15	0.020 ±0.009	0.37 ±0.053	0.084 ±0.017	10.5 ±2.05	4.7 ±1	2.1 ±0.9	27.8 ±8.2
CLI	5.9 ±0.26	0.044 ±0.013	0.53 ±0.131	0.057 ±0.007	9.2 ±1.7	4.0 ±0.6	1.0 ±0.7	18.7 ±6.2
LFI	6.1 ±0.2	0.006 ±0.003	2.56 ±0.979	0.154 ±0.055	17.1 ±4.5	6.6 ±1.35	0.5 ±0.4	36.3 ±4.2
NV	5.1 ±0.1	0.002 ±0.0005	0.25 ±0.07	0.184 ±0.067	3.6 ±0.87	2.7 ±0.52	8.5 ±1.8	26.2 ±3.7
NT	5.4 ±0.2	0.029 ±0.009	0.49 ±0.102	0.019 ±0.011	6.9 ±2.5	3.1 ±0.7	3.3 ±3	26.5 ±3.24
0.20–0.40 m								
CFI	5.3 ±0.15	0.006 ±0.004	0.31 ±0.08	0.118 ±0.108	4.4 ±0.76	3.0 ±0.5	8.0 ±1.9	22.3 ±0.4
CLI	5.3 ±0.20	0.027 ±0.008	0.46 ±0.15	0.054 ±0.036	5.1 ±1.8	2.9 ±0.3	4.3 ±1.7	15.3 ±4.5
LFI	5.5 ±0.19	0.005 ±0.003	0.76 ±0.51	0.079 ±0.091	9.9 ±3.7	4.6 ±1.3	4.4 ±3.1	34.6 ±2.3
NV	5.1 ±0.18	0.001 ±0.0004	0.21 ±0.16	0.191 ±0.12	2.7 ±0.84	2.3 ±0.6	7.7 ±1.3	24.4 ±3.3
NT	5.2 ±0.16	0.014 ±0.009	0.44 ±0.13	0.020 ±0.004	4.1 ±2.45	2.6 ±0.6	6.1 ±2.4	21.2 ±0.8

* CFI—Crop–Forest Integration; CLI—Crop–Livestock Integration; LFI—Livestock–Forest integration; NV—native vegetation; NT—no-till farming system. Legend: pH—hydrogen potential; P—phosphorus; K+—potassium; Na^+—sodium; Ca^{2+}—calcium; Mg^{2+}—magnesium; Al^{3+}—aluminum; SOM—soil organic matter.

Table 2. Physical characterization and total organic carbon of a typical dystrocohesive Yellow Argisol (Ultisol) under different management systems in the Cerrado of Maranhão, Brazil.

Land Use *	Sand	Clay	Silt	TOC		Bd		SCS	
	g · kg^{-1}			dag · kg^{-1}		kg · m^{-3}		Mg · ha^{-1}	
0–0.10 m									
CFI	722	148	130	1.59	±0.47	1.62	±0.47	24.50	±8.5
CLI	734	153	113	1.20	±0.41	1.72	±0.41	21.70	±7
LFI	669	198	133	2.02	±0.28	1.57	±0.28	32.70	±3.59
NV	701	150	149	1.57	±0.22	1.62	±0.22	24.20	±3.12
NT	744	156	100	1.52	±0.28	1.61	±0.28	22.80	±2.59
0.10–0.20 m									
CFI	712	178	110	1.47	±0.44	1.72	±0.08	23.50	±6.62
CLI	697	194	109	0.87	±0.29	1.83	±0.04	16.70	±5.71
LFI	669	204	127	1.68	±0.19	1.68	±0.08	29.10	±3.51
NV	639	189	172	1.41	±0.17	1.55	±0.17	21.60	±4.14
NT	680	186	134	1.39	±0.2	1.69	±0.08	23.50	±3.21
0.20–0.40 m									
CFI	672	218	110	1.18	±0.02	1.72	±0.03	40.60	±1.91
CLI	686	238	76	0.71	±0.21	1.85	±0.08	25.50	±6.12
LFI	655	254	91	1.60	±0.11	1.50	±0.07	48.40	±5.64
NV	711	222	67	1.12	±0.04	1.55	±0.13	33.10	±4.34
NT	711	189	100	1.29	±0.17	1.60	±0.22	45.10	±6.58

* CFI—Crop–Forest Integration; CLI—Crop–Livestock Integration; LFI—Livestock–Forest integration; NV—native vegetation; NT—no-till farming system. Legend: TOC—soil organic carbon; Bd—soil bulk density; SCS—soil carbon stock.

For the determination of soil water retention curves, undisturbed soil samples were collected using volumetric rings with a volume of 98.17 cm^3, extracted with the aid of a "castelinho"-type auger. Mini-trenches were opened at four randomly selected points within each management system, and samples were collected at depths of 0.00–0.10, 0.10–0.20, and 0.20–0.40 m (Figure 2).

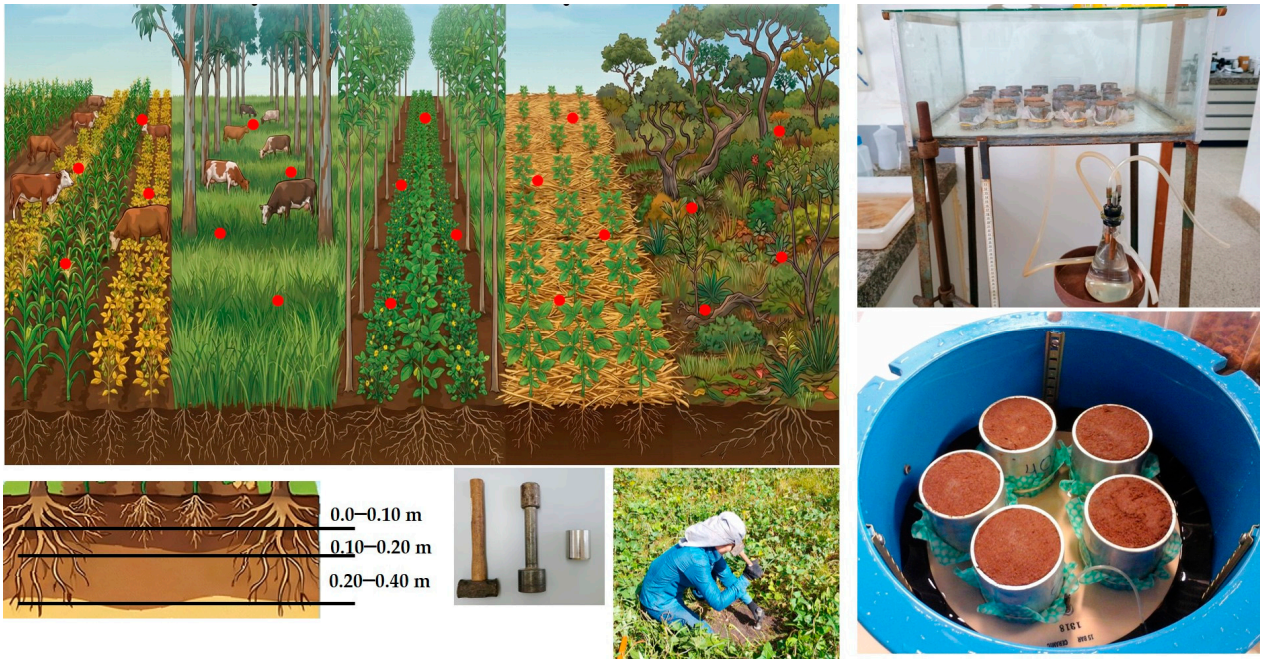

Figure 2. Sampling scheme for undisturbed soil samples (red points indicate the sampling sequence); soil layers, instruments, and sampling procedure; tension table and Richards pressure chamber used to determine the soil water retention curve.

2.3. Determination of Water Retention Curves

Soil water retention curves were determined using tension tables and Richards pressure chambers. The matric potentials applied on the tension tables were 0.5, 2, 4, 6, and 10 kPa, whereas pressures of 500 and 1500 kPa were applied in the pressure chambers.

The samples were saturated with distilled water for 24 h and subsequently placed on the tension tables and in the pressure chambers, where suction (on the tension tables) or air pressure (in the chambers) corresponding to the target matric potential was applied. This procedure promoted drainage of the soil solution from the samples until equilibrium was reached, that is, when water flow ceased and the matric potential equilibrated the applied suction (h) or air pressure (P). Once equilibrium was attained on the tension tables and in the pressure chambers, the samples were weighed on an analytical balance with 0.01 g precision to obtain the wet mass (MU). Subsequently, the samples were oven-dried in a forced-air circulation oven at 105 °C for 48 h. After drying, the samples were weighed again to determine the dry mass (MS). Based on these measurements, soil bulk density (Bd) (Equation (1)) and gravimetric (U) and volumetric (θ) water contents were calculated according to Equations (2) and (3), respectively.

$$\mathrm{Bd} = \mathrm{MS/V}\ (\mathrm{Kg} \cdot \mathrm{m}^{-3}) \tag{1}$$

$$\mathrm{U} = (\mathrm{MU} - \mathrm{MS})/\mathrm{MS}\ (\mathrm{Kg} \cdot \mathrm{Kg}^{-1}) \tag{2}$$

$$\theta = (\mathrm{U.Bd})/1000\ (\mathrm{m}^3 \cdot \mathrm{m}^{-3}), \tag{3}$$

where V is the volume of the soil core cylinder (m^3) and 1000 is the density of water ($kg \cdot m^{-3}$). The data were fitted to the model proposed by van Genuchten [36], Equation (4):

$$\theta = \theta r + ((\theta s - \theta r)/\ ((1 + (\alpha \cdot\ |\phi m|\hat{}n))\hat{}m)), \tag{4}$$

where θr and θs ($m^3 \cdot m^{-3}$) are the residual and saturated water contents, respectively; ϕm is the soil water matric potential (tension); and α, n, and m are fitting parameters of the

equation. The parameters α and n define the shape of the curve, where α is the inverse of the air-entry potential (kPa^{-1}), n represents the influence of pore-size distribution on the slope of the soil water retention curve, and m depends on the value of n ($m = 1 - 1/n$).

The fitting of the data to Equation (4) was performed using the TableCurve 2D Version 5.01 software. To evaluate differences among the water retention curves across management systems and soil layers, 95% confidence intervals were plotted. Curves were considered similar when their confidence bands overlapped; in the absence of overlap, the curves were considered statistically distinct.

2.4. Field Capacity, Permanent Wilting Point, and Soil Available Water (AW)

Saturated water content (θs) was obtained from the mass of the sample prior to the application of suction on the tension table or air pressure in the pressure chambers. At this stage, the entire pore volume of the sample was filled with water; therefore, this water content was considered equivalent to the total porosity (*TP*) of the sample. Field capacity (θfc) and the permanent wilting point (θpwp) were defined as the water contents retained at matric potentials of 10 kPa and 1500 kPa, respectively. Soil available water (*AW*) was calculated as the difference between θfc and θpwp, according to Equation (5):

$$\mathrm{AW} = \theta\mathrm{fc} - \theta_{\mathrm{PWP}}\ (\mathrm{m}^3 \cdot \mathrm{m}^{-3}) \quad (5)$$

The mean values of θs, θfc, θpwp, and *AW* were subjected to analysis of variance (ANOVA) to assess differences among soil layers within each management system. The application of ANOVA considered data normality (Shapiro–Wilk test, $p > 0.05$) and homogeneity of variances (Levene's test, $p > 0.05$). When statistical significance was detected ($p < 0.05$), means were compared using Tukey's test at the 5% probability level.

2.5. Pore-Size Distribution

Soil pore-size distribution was determined based on the fitted soil water retention curves, using capillarity theory as a basis [37]. According to this theory, the soil solution–air interfaces within pores are characterized by their curvature radius (R). Thus, the soil water matric potential can be related to the equivalent pore radius (r) (Equations (6) and (7)):

$$\Phi\mathrm{m} = \mathrm{h} = 2\sigma\cos\alpha/\mathrm{d}_{\mathrm{sol}}\mathrm{gr}\ (\mathrm{energy/weight} \equiv \mathrm{m}) \quad (6)$$

and

$$\Phi\mathrm{m} = \mathrm{P} = 2\sigma\cos\alpha/\mathrm{r}\ (\mathrm{energy/solution\ volume} \equiv \mathrm{Pa}), \quad (7)$$

where ϕm is the matric potential; h is the height set on the tension table; P is the air pressure applied in the pressure chamber; σ (0.07275 N m^{-1}) is the surface tension of the soil solution at 25 °C; α is the angle formed between the tangent line at the triple contact point (pore–air–water) and the pore wall; g is the acceleration due to gravity; and d_{sol} is the density of the soil solution.

Based on these relationships, soil pore-size distribution was obtained considering the following limits [38]: pores with radii smaller than 15 μm (equivalent to 3 kPa) were classified as micropores; those with radii between 15 and 50 μm (between 3 and 10 kPa) as mesopores; and pores with radii larger than 50 μm as macropores.

By differentiating the soil water retention curve for each management system and soil layer, the cumulative frequency of pore radius on a logarithmic scale was obtained. For this purpose, Equation (4) was rearranged so that the function became θ(r) (Equation (8),

with $R = r$ or $cos\ \alpha = 1$), and subsequently differentiated (Equation (10)) to obtain the most frequent pore radius (*Rmax*), according to Equation (11) [39]:

$$\theta = \theta + ((\theta s - \theta r)/(1 + (A/r)\hat{}n)\hat{}m)) \quad (8)$$

$$A = 2\sigma\alpha 10^3 \quad (9)$$

$$d\theta/d\log r = (\theta s - \theta r) \cdot m \cdot n \cdot A\hat{}n \cdot r\hat{}{-}n \cdot (1 + A\hat{}nr\hat{}{-}n)\hat{}m{-}1 \quad (10)$$

$$Rmax = (A(1/m))\hat{}(-1/n) \quad (11)$$

The frequency curves of pore radius per logarithmic interval of *r*, obtained by the differentiation of the fitted soil water retention equations, represent the soil pore-size distribution by indicating the number of pores within each size class and enabling the identification of predominant pore classes. The peaks of these curves correspond to the most frequent pore sizes (*Rmax*), whereas the position and shape of the distribution reflect soil structure. Curves concentrated at higher log(*r*) values indicate a predominance of macropores, which are associated with greater drainage capacity. In contrast, curves shifted toward lower values indicate a predominance of micropores, which are associated with higher water retention. Therefore, the analysis of these frequency curves enables a better understanding of soil hydrological behavior and water storage capacity.

2.6. Relative Soil Hydraulic Conductivity (Kr)

Relative soil hydraulic conductivity (*Kr*) was derived from the soil water retention curve using the Mualem–van Genuchten mathematical model (Equation 12). Van Genuchten [36] employed Equation (4) to fit the water retention curve and, based on this formulation, obtained an analytical solution of the relative hydraulic conductivity expression developed by Mualem [40], assuming the dependency $m = 1 - 1/n$ between the fitted parameters of the equation:

$$Kr = (Se\hat{}l)(1 - (1 - (Se\hat{}(1/m))\hat{}m))\hat{}2 \quad (12)$$

$$Se = (\theta(\phi m) - \theta r)/(\theta s - \theta r), \quad (13)$$

where θ is the volumetric water content ($m^3 \cdot m^{-3}$) at a given matric potential (ϕm); θr and θs are the residual and saturated water contents, respectively ($m^3 \cdot m^{-3}$); and l is an empirical parameter related to pore connectivity, fixed by Mualem [40] at *0.5*.

3. Results

3.1. Soil Water Retention Curves

The soil water retention curves determined for the CFI, CLI, LFI, NV, and NT systems at soil depths of 0.00–0.10 m (Figure 3A), 0.10–0.20 m (Figure 3B), and 0.20–0.40 m (Figure 3C) show shaded bands representing the 95% confidence intervals. These confidence bands allowed the curves to be statistically distinct when no overlap occurred or statistically similar when overlap occurred. The fitted parameters of the curves are presented in Table 3.

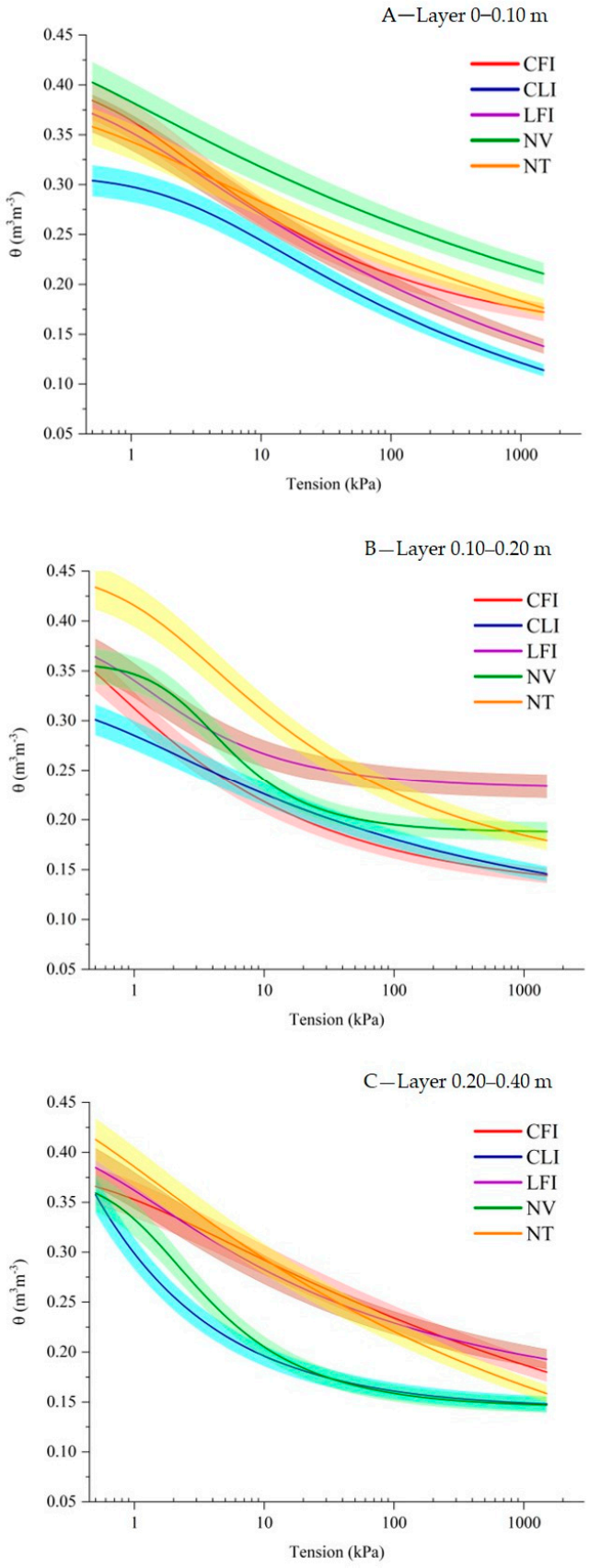

Figure 3. Soil water retention curves and confidence intervals (shades of the same color as the curve) for the following systems: CFI—Crop–Forest Integration; CLI—Crop–Livestock Integration; LFI—Livestock–Forest Integration; NV—native vegetation; NT—no-till farming system.

Table 3. Fitted parameters, ±standard error (confidence intervals 95%), of the soil water retention'curves.

Fitted Parameters *	CFI		CLI		LFI		NV		NT	
	0–0.10 m									
θ_r ($m^3 \cdot m^{-3}$)	0.15	±0.053 (0.02)	0.11	±0.31 (0.02)	0.13	±0.21 (0.02)	0.21	±0.33 (0.04)	0.14	±0.42 (0.02)
θ_s ($m^3 \cdot m^{-3}$)	0.41	±0.036 (0.15)	0.31	±0.01 (0.08)	0.4	±0.04 (0.12)	0.45	±0.13 (0.55)	0.38	±0.05 (0.22)
α (kPa^{-1})	1.16	±1.6 (6.53)	0.39	±0.7 (0.75)	1.73	±3.02 (3.4)	6.2	±31.6 (12.4)	2.45	±7.56 (4.8)
n	1.28	±0.2 (0.83)	1.16	±0.28 (1.14)	1.14	±0.14 (0.57)	1.09	±0. 13 (0.56)	1.09	±0.17 (0.72)
R^2	0.91		0.9		0.95		0.95		0.92	
	0.10–0.20 m									
θ_r ($m^3 \cdot m^{-3}$)	0.19	±0.95 (0.08)	0.17	±0.18 (0.02)	0.23	±0.006 (0.03)	0.18	±0.006 (0.03)	0.13	±0.009 (0.28)
θ_s ($m^3 \cdot m^{-3}$)	0.31	±0.012 (0.07)	0.33	±0.09 (0.39)	0.39	±0.03 (0.11)	0.36	±0.01 (0.04)	0.45	±0.04 (0.16)
α (kPa^{-1})	0.01	±0.06 (0.24)	2.33	±10.8 (4.6)	1.44	±1.23 (2.88)	0.37	±0.11 (0.46)	0.78	±1.12 (1.56)
n	1.1	±3.85 (15.85)	1.17	±0.32 (1.3)	1.56	±0.18 (0.78)	1.86	±0.24 (1.01)	1.29	±0.27 (1.13)
R^2	0.61		0.77		0.92		0.93		0.87	
	0.20–0.40 m									
θ_r ($m^3 \cdot m^{-3}$)	0.16	±0.21 (0.06)	0.14	±0.023 (0.09)	0.15	±0.05 (0.2)	0.14	±0.011 (0.02)	0.15	±0.15 (0.04)
θ_s ($m^3 \cdot m^{-3}$)	0.39	±0.018 (0.08)	0.39	±0.02 (0.07)	0.42	±0.05 (0.2)	0.38	±0.024 (0.10)	0.47	±0.12 (0.5)
α (kPa^{-1})	1.68	±1.96 (3.36)	0.98	±0.67 (1.96)	2.45	±4.35 (4.9)	0.83	±0.48 (1.67)	4.44	±14.8 (8.9)
n	1.1	±0.087 (0.36)	1.31	±0.12 (0.05)	1.22	±0.13 (0.55)	1.63	±0.21 (0.27)	1.13	±0.12 (0.53)
R^2	0.98		0.97		0.95		0.91		0.95	

* θs—saturated water content; θr—residual water content; α and n—parameters of the equation; R^2—coefficient of determination; CFI—Crop–Forest Integration; CLI—Crop–Livestock Integration; LFI—Livestock–Forest integration; NV—native vegetation; NT—no-till farming system.

The soil water retention curves obtained for the CFI, LFI, and NT systems in the 0.00–0.10 m layer did not differ from each other over most of their extent (Figure 3A). The NV and CLI curves did not show an overlap of confidence intervals with the others; however, while NV retained higher water contents at all applied matric potentials, CLI exhibited lower water contents, with a gradient of approximately 0.10 $m^3 \cdot m^{-3}$ relative to NV. At higher matric suctions (500 and 1500 kPa), the curves showed distinct behavior, with water retention decreasing in the following order: NV > NT and CFI > LFI > CLI. This demonstrates the influence of the evaluated systems on water retention under drier soil conditions.

In the 0.10–0.20 m layer (Figure 3B), up to a matric potential of 10 kPa, the NT retention curve differed from the others, showing the highest saturated water content (θs = 0.45 $m^3 \cdot m^{-3}$) among all systems. Subsequently, the NV, LFI, and CFI curves were similar to each other (θs values of 0.36, 0.39, and 0.35 m^3 m^{-3}, respectively), whereas CLI showed the lowest water contents in the initial portion of the retention curve (θs = 0.33 $m^3 \cdot m^{-3}$). From a matric potential of 100 kPa onward, a range in which water retention becomes primarily controlled by soil texture, the LFI system exhibited higher water contents. At higher matric potentials, the NT and NV curves overlapped, while CFI and CLI showed lower water contents. In the 0.20–0.40 m layer (Figure 3C), the NT, LFI, and CFI systems differed from CLI and NV, with the former retaining higher water contents at all matric potentials.

Soil water retention curves varied across the analyzed soil layers for each land-use system, highlighting distinct hydraulic behaviors throughout the profile. Native vegetation (NV) exhibited higher water content in the surface layer (0.00–0.10 m) compared to the other systems. However, in the deeper layers, water retention in NV was lower than that observed in NT and LFI at 0.10–0.20 m, and lower than NT, CFI, and LFI at 0.20–0.40 m. The higher retention of NV in the surface layer is associated with continuous litter in-

put, which provides soil protection, enhances biological activity, and promotes structural improvements consolidated by the absence of anthropogenic intervention.

The evaluated soils exhibit a cohesive character, with naturally dense subsurface layers. This condition, combined with the sandy texture, likely contributed to the lower water retention in the subsurface, particularly in the native vegetation (NV) environment. In contrast, the NT system showed increased water retention in the 0.10–0.20 m layer, possibly due to long-term conservation practices. These practices favored higher organic matter content and the development of structural pores, which are essential for soil water retention.

The integrated systems CFI and LFI also showed increased water retention in the subsurface layers. In the LFI system, the continuous presence of grasses contributed to higher water content in the 0.10–0.20 m layer, particularly at higher matric suctions. However, at the 0.20–0.40 m depth, the behavior was similar to the other systems, likely due to the natural soil densification at this depth. The CLI system exhibited the least variation in water retention across the profile. This may be explained by its land-use history, characterized by a short period of livestock integration, recent soil disturbance, and a history of soybean monoculture for several years prior to the implementation of the integrated system.

3.2. Field Capacity, Permanent Wilting Point, and Soil Available Water

Field capacity (θfc), permanent wilting point (θpwp), and soil available water (AW) are hydraulic properties derived from the soil water retention curve and may vary according to soil type, management system, and the soil layer evaluated (Table 4). In the surface soil layer (0.00–0.10 m), the CLI system exhibited lower values of θs (0.309 $m^3 \cdot m^{-3}$), θfc (0.240 $m^3 \cdot m^{-3}$), and θpwp (0.108 $m^3 \cdot m^{-3}$) than all other systems, reflecting the behavior of the soil water retention curve under this management (Figure 3A). The NV system showed the highest θfc (0.304 $m^3 \cdot m^{-3}$) and θpwp (0.212 $m^3 \cdot m^{-3}$), thereby reducing AW (0.10 $m^3 \cdot m^{-3}$) in this system. In the subsequent layers (0.10–0.20 and 0.20–0.40 m), only the NT system stood out, exhibiting higher AW values (0.128 and 0.136 $m^3 \cdot m^{-3}$, respectively).

Table 4. Saturated water content (θs), field capacity (θfc), permanent wilting point (θpwp), and available soil water (AW) for the evaluated systems and soil layers.

Land Use *	θs		Θfc		θpwp		AW	
	$m^{-3} \cdot m^{-3}$							
	0–0.10 m							
CFI	0.383 a	±0.032	0.263 bc	±0.01	0.149 b	±0.015	0.114	±0.020
CLI	0.309 b	±0.029	0.240 c	±0.011	0.108 c	±0.019	0.132	±0.011
LFI	0.371 a	±0.025	0.267 b	±0.016	0.135 bc	±0.001	0.132	±0.014
NV	0.402 a	±0.015	0.304 a	±0.011	0.212 a	±0.014	0.092	±0.021
NT	0.36 ab	±0.007	0.277 b	±0.01	0.144 b	±0.013	0.133	±0.008
F test	8.26		14.66		23.81		3.1	
p value	0.009 **		0.001 **		<0.001 **		0.088 ns	
	0.10–0.20 m							
CFI	0.348 b	±0.021	0.286 b	±0.011	0.193 b	±0.003	0.092 b	±0.012
CLI	0.301 b	±0.016	0.239 c	±0.016	0.172 c	±0.006	0.066 b	±0.012
LFI	0.364 ab	±0.015	0.254 cd	±0.003	0.223 a	±0.014	0.032 c	±0.017
NV	0.356 ab	±0.020	0.228 d	±0.007	0.178 bc	±0.005	0.05 c	±0.005
NT	0.431 a	±0.072	0.313 a	±0.006	0.185 bc	±0.010	0.128 a	±0.012
F test	8.29		76.86		13.24		32.61	
p value	0.008 **		<0.001 **		0.002 **		<0.001 **	

Table 4. *Cont.*

Land Use *	*θs*		*Θfc*		*θpwp*		*AW*	
	$m^{-3} \cdot m^{-3}$							
0.20–0.40 m								
CFI	0.367	±0.009	0.253 b	±0.01	0.161 ab	±0.001	0.092 b	±0.008
CLI	0.362	±0.016	0.210 bc	±0.025	0.137 bc	±0.024	0.073 b	±0.004
LFI	0.384	±0.009	0.269 ab	±0.009	0.178 a	±0.003	0.091 b	±0.012
NV	0.358	±0.048	0.209 c	±0.007	0.124 c	±0.014	0.085 b	±0.018
NT	0.412	±0.034	0.289 a	±0.0002	0.153 b	±0.007	0.136 a	±0.007
F test	2.88		123.92		24.54		51.88	
p value	0.104 ns		< 0.001 **		< 0.001 **		< 0.001 **	

* CFI—Crop–Forest Integration; CLI—Crop–Livestock Integration; LFI—Livestock–Forest integration; NV—native vegetation; NT—no-till farming system. Legend: **, significant at 1% ($p < 0.01$); ns, not significant; means followed by the same letter in the column do not differ significantly by Tukey's test; multiple comparisons were performed only when ANOVA indicated a significant overall effect.

3.3. Pore-Size Distribution

Pores were classified according to their radius (Table 5) based on the calculation of the equivalent pore radius derived from the soil water retention curves. In all soil layers and management systems evaluated, micropores predominated. The CLI system, in the two upper layers (0.00–0.10 and 0.10–0.20 m), showed reduced total porosity compared with the other systems (0.31 and 0.30 $m^3 \cdot m^{-3}$, respectively). Although the proportions of macro-, meso-, and micropores among the systems were similar, the lower total porosity in the CLI system may have affected its overall water retention capacity.

Table 5. Total porosity (TP), macro-, meso-, and microporosity and the most frequent pore radius (*Rmax*) of an Argisol under integrated production systems, a no-tillage system, and native Cerrado vegetation.

Land Use	TP	Macropores	Mesopores	Micropores	*Rmax*
	$m^3 \cdot m^{-3}$	%			µm
CFI	0.38	18.02	11.68	70.30	51.33
CLI	0.31	9.77	10.81	79.42	10.11
LFI	0.37	16.78	11.15	72.07	38.74
NV	0.40	13.82	7.81	78.37	96.15
NT	0.36	12.60	8.97	78.43	38.22
0.10–0.20 m					
CFI	0.35	8.82	5.64	85.53	40.24
CLI	0.30	16.08	9.48	74.45	66.39
LFI	0.36	18.63	8.07	73.31	108.55
NV	0.36	15.96	17.13	66.91	35.88
NT	0.43	32.37	16.86	50.77	110.70
0.20–0.40 m					
CFI	0.37	12.22	8.54	79.24	26.95
CLI	0.36	17.41	11.74	70.85	48.07
LFI	0.38	16.96	10.20	72.84	89.30
NV	0.36	28.00	15.70	56.31	67.47
NT	0.41	19.04	10.59	70.37	96.32

CFI—Crop–Forest Integration; CLI—Crop–Livestock Integration; LFI—Livestock–Forest integration; NV—native vegetation; NT—no-till farming system.

In the 0.00–0.10 m layer, the most frequent pore radii (*Rmax*) were within the macropore range for CFI and NV (51.33 and 96.15 µm, respectively), within the mesopore range for

LFI and NT (38.74 and 38.22 μm, respectively), and within the micropore range for CLI (10.11 μm). In the 0.10–0.20 m layer, a reduction in the proportion of micropores was observed for most systems, except for CFI, which showed a high proportion of micropores (85.53%) and a considerable reduction in the proportions of macro- and mesopores (8.82 and 5.64%, respectively), with *Rmax* concentrated in the mesopore range. In the 0.20–0.40 m layer, only the NT system showed an increase in micropores (70.37%); for the other systems, an increase in the proportion of macropores was observed, with *Rmax* occurring within the macropore range.

The frequency curves of pore radii per *log*(*r*) interval, derived from the soil water retention curves for the studied management systems and soil layers, enabled the separation of pore classes (macro-, meso-, and micropores) (Figure 4A–C). The yellow band of the graph represents the frequency of micropores ($r < 15$ μm), the white band represents mesopores ($15 < r < 50$ μm), and the blue band represents macropores ($r > 50$ μm).

In the 0.00–0.10 m layer, the pore-radius frequency curve per *log*(*r*) interval for the CLI system (Figure 4A) showed a peak shifted toward the yellow band of the graph, indicating that the most frequent pore radii are concentrated in the micropore range. The curves for the CFI and LFI systems exhibited peaks in the white band, corresponding to mesopores, whereas the curves for the NV and NT systems showed peaks in the blue portion of the graph, with the most frequent pore radii in the macropore range.

In the 0.10–0.20 m layer, the pore-radius frequency curves for the NV and NT systems (Figure 4B) displayed higher peaks concentrated in the white band of the graph (mesopores), indicating that pores are more readily associated with drainage. In contrast, the curve for the LFI system was shifted toward the blue band (macropores) and exhibited a lower peak, indicating a higher proportion of micropores compared with the previous systems. The curves for the CFI and CLI systems showed the lowest peaks, indicating a predominance of micropores; however, these peaks were shifted toward the blue band, meaning that the most frequent pore radius occurred within the macropore range.

In the 0.20–0.40 m layer (Figure 4C), the curve for the NV system exhibited a higher peak shifted toward the blue portion of the graph, indicating that the most frequent pore radius was within the macropore range. The curve for the CLI system showed a peak in the white band of the graph (mesopores), whereas for the CFI, LFI, and NT systems, the peaks were shifted toward the blue band (macropores); however, because these peaks were less pronounced, these systems exhibited a higher proportion of micropores compared with the NV system.

3.4. Relative Soil Hydraulic Conductivity

Relative soil hydraulic conductivity (*Kr*) ranges from 0 to 1 (Figure 5A–C), with $Kr = 1$ when the soil is saturated (all pores filled with water) and decreasing as the soil dries. For each management system, a *log* $Kr(\theta)$ curve was generated based on the fitted water retention curves and within the range of water contents obtained for each system (θs and θr). In general, systems with a higher proportion of micropores exhibited *log Kr* curves that decreased more gradually, that is, with a more horizontal shape.

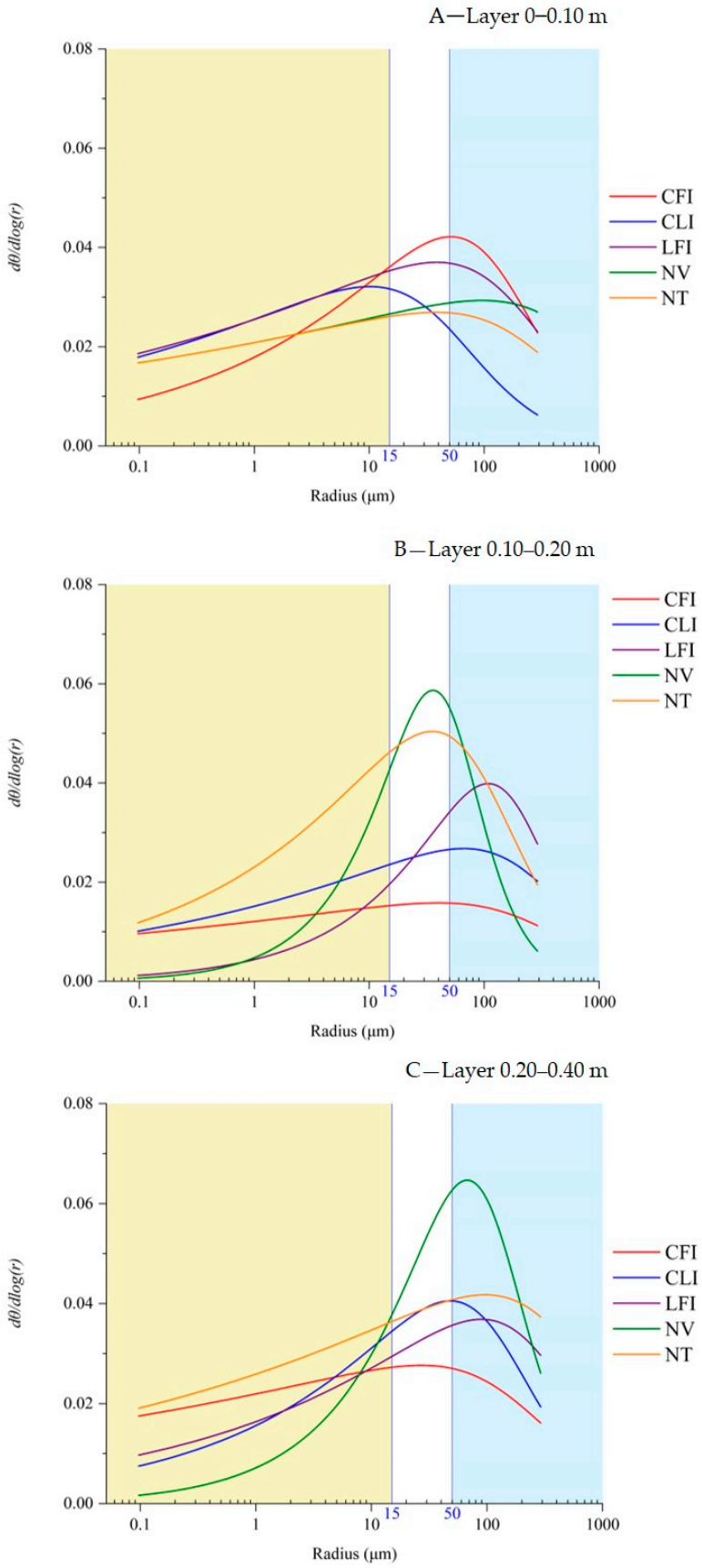

Figure 4. Pore-radius frequency function curves per logarithmic interval of r highlighting micropores (yellow zone), mesopores (white zone), and macropores (blue zone). Systems: CFI—Crop–Forest Integration; CLI—Crop–Livestock Integration; LFI—Livestock–Forest Integration; NV—native vegetation; NT—no-till farming system.

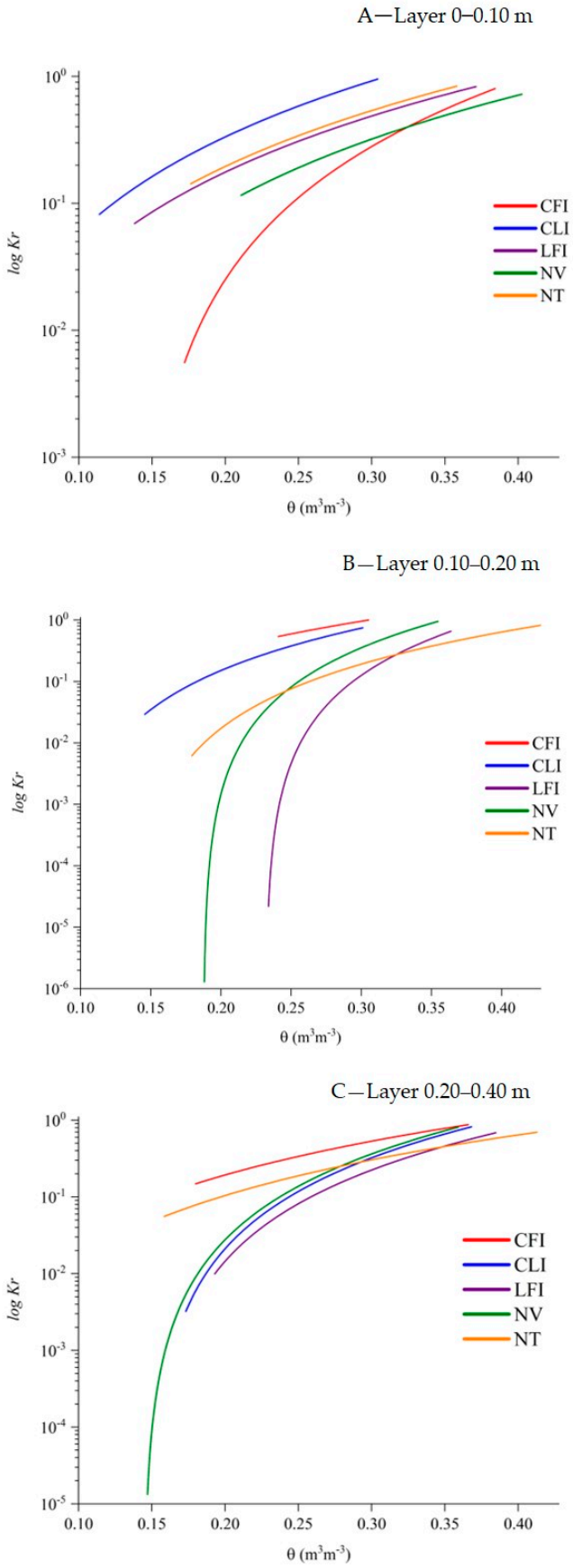

Figure 5. Relative soil hydraulic conductivity (*log Kr*) as a function of soil water content (θ). Systems: CFI—Crop–Forest Integration; CLI—Crop–Livestock Integration; LFI—Livestock–Forest Integration; NV—native vegetation; NT—no-till farming system.

Overall, the CLI system (Figure 5) exhibited *log Kr* values with little variation, decreasing gradually over the analyzed range of water contents, resulting in a more horizontal curve. In contrast, the NV system showed faster and more efficient drainage of soil pores, reflected by a greater variation in *log Kr*.

In the surface layer (0.00–0.10 m), the CFI system (Figure 5A) showed the greatest variation in *log Kr*, indicating more dynamic water movement, with higher values at greater water contents (macropores and mesopores) and a sharp decrease as the soil dried. However, in the subsequent layer (0.10–0.20 m), the CFI and CLI systems (Figure 5B) exhibited curves with little variation in *log Kr*, whereas the NT, NV, and LFI systems showed curves with a rapid decrease in *log Kr* as water content declined. In the 0.20–0.40 m layer (Figure 5C), the CFI and NT systems displayed more horizontal *log Kr* curves, indicating slower pore drainage, while the NV, CLI, and LFI systems showed a more rapid reduction in *Kr* over the analyzed water content range.

4. Discussion

4.1. Soil Water Retention Curves

The CFI, LFI, and NT systems showed higher soil water retention, being lower than the native vegetation (NV) only in the surface layer. This behavior can be attributed to the adoption of conservation practices, such as the absence of soil disturbance, plant species diversity, and the continuous input of organic residues, which favor the formation and structural stability of aggregates. Soil organic matter (SOM) plays a central role in this process by contributing to the formation, stabilization, and connectivity of structural pores, which are responsible for water retention after the free drainage of a saturated soil. Furthermore, SOM increases the negative charges on colloids, intensifying the adsorption of water molecules [13,14,24–26].

Among the integrated systems, CFI and LFI showed higher retained water content, being surpassed only by NT in the 0.10–0.20 m layer. These systems are characterized by a diversified land-use history involving annual crop and grass rotation, maintenance of soil cover, and livestock grazing during specific periods of the year. The presence of grasses favored an increase in SOM content (Table 2) which, combined with their fibrous root systems, contributed to improved soil structure. Additionally, maintaining soil surface cover reduced water loss to the atmosphere. Another relevant aspect is the presence of the forest component in both systems, which promoted continuous litterfall (leaves and branches), increasing SOM levels and diversifying biological activity. Together, these factors were decisive in increasing soil structural stability and, consequently, enhancing water retention in the CFI and LFI systems.

The NT system exhibited the highest water retention, especially in the 0.10–0.20 m layer, compared to the other evaluated systems. This area was established in 2005 and has been maintained to the present, featuring permanent soil cover, continuous organic residue input, and no soil disturbance. These conditions favored the stabilization of the soil pore structure, characterized by greater pore continuity and a more balanced distribution among macro-, meso-, and micropores, thus increasing storage capacity and water availability for plants. Additionally, permanent soil surface cover contributed to reducing water loss through evaporation and maintaining milder soil temperatures compared to exposed soils. These factors are reflected not only in higher retained water content but also in greater resistance to erosive processes, with positive effects on soil water infiltration and permeability.

Among the evaluated systems, CLI exhibited the lowest water retention across all soil layers. At the time of this study (2024), this system had been established for only two years and was preceded by management practices characterized by intense soil disturbance, limited plant diversity, and low organic matter inputs—namely, 17 years of soybean

monoculture—resulting in the lowest total organic carbon contents (Table 2). In addition, the studied soil has a high sand fraction, which, combined with the recent establishment of the system, limited SOM accumulation and hindered improvements in soil water retention. Thus, the brief establishment period of the CLI system was insufficient to promote structural improvements through SOM accumulation and to enhance soil water retention.

The differences in water retention among soil layers across the evaluated systems are primarily associated with the vertical distribution of organic matter, land-use history, and modifications in soil structure throughout the profile. The surface layers—especially in NV and systems with higher residue input (NT, LFI, and CFI)—exhibited higher water retention due to litter accumulation, crop diversity (including grasses, forest species, and annual/forage crop rotations), increased biological activity, and improved soil aggregation. In the subsurface, water retention was conditioned by the degree of natural densification, sandy texture, and the presence of structural pores formed over time under conservation practices such as no-tillage, permanent cover, and plant diversification. Systems with longer adoption times and continuous conservation management favored the stabilization of the pore structure and improved pore connectivity, resulting in greater water storage capacity in deeper layers. In contrast, systems with recent adoption or a history of soil disturbance showed less hydric differentiation across the analyzed soil layers.

Physical soil restructuring, particularly via organic carbon accumulation, is a time-dependent process. Even sustainable management systems such as Crop–Livestock–Forest Integration may not show significant improvements—or may even exhibit initial declines—when adopted for short periods. In a short-term study evaluating the impact of implementing a Crop–Livestock–Forest system in Cerrado soils of Central Brazil, physical degradation was observed after only two years of adoption in a Ferralsol [9], with lower organic matter content, reduced soil aeration capacity, and a lower S index (an indicator of soil physical quality) relative to a reference pasture. Another study assessing the transition from degraded pasture to Crop–Livestock Integration systems in sandy soils in Brazil reported, after three years of implementation, a decline in soil health indicators compared with pasture and native vegetation. This reduction was attributed to decreases in biological components, notably soil organic carbon and β-glucosidase activity, leading to "stress" on biological components during the early stages of system establishment, when soil structure and microbial communities were still adapting to new land-use practices [20].

The CFI, LFI, and NT systems stood out for higher water retention, with values lower than those of native vegetation (NV) only in the surface layer. In the CFI and LFI systems, higher total organic carbon contents (Table 2) likely contributed to increased water retention. Specifically in the CFI system, the presence of grasses likely enhanced organic matter inputs, while in both systems the eucalyptus tree rows may also have played an important role in increasing total organic carbon and, consequently, soil water retention compared with the CLI system. The NT system, with 19 years of continuous adoption, showed high θs values, particularly in the intermediate layer (0.10–0.20 m). Thus, long-term no-tillage management—with permanent soil cover and the absence of mechanical disturbance—contributed to increasing soil water storage capacity and water availability of plants (Table 4). This condition may also enhance resistance to erosion processes and, consequently, improve water infiltration and soil permeability.

The adoption of sustainable and regenerative management systems, such as Integrated Crop–Livestock–Forest (ICLF) systems and their arrangements, has demonstrated the capacity to increase soil water retention—a benefit closely linked to increases in soil organic carbon and improvements in soil structure [15,19,22,30,32,41]. Long-term studies in Brazil have reported significant improvements in water retention and storage, as well as enhanced soil structural stability, under Crop–Livestock and Crop–Livestock–Forest

Integration systems on degraded soils [15]. In sandy soils, increases in soil organic carbon resulting from the adoption of integrated systems have produced marked benefits for water retention, leading to higher estimates of gravimetric moisture and infiltration, surpassing other systems and approaching values observed under native vegetation [22]. A study conducted on a sandy Cambisol in the Brazilian Cerrado found that a Crop–Livestock–Forest Integration system between tree rows exhibited higher plant-available water capacity than a reference pasture, which was attributed to higher organic matter content [9]. Overall, the integration of crops, livestock, and forest components promotes increases in soil organic carbon, improves soil structure and aggregation, and consequently enhances soil water retention [15].

4.2. Pore-Size Distribution

Overall, the curves of the pore-radius frequency function per logarithmic interval of r for the evaluated systems and soil layers, characterized by curve peaks within the macro- and mesopore ranges, indicate that the studied systems—by increasing and diversifying organic matter inputs to the soil—contributed to stabilizing soil pore geometry, thereby improving water and air fluxes. Except for the surface layer, the leftward shift in the curve peak in the CLI system reflects a higher frequency of micropores, likely due to the land-use history that caused surface soil degradation. In contrast, in the 0.10–0.20 m layer, the higher and narrower curves observed for the NV and NT systems stood out, indicating a complex and stabilized structural organization, with the most frequent pore radii occurring within the macropore range, including aeration and rapid drainage pores, as well as capillary water retention pores.

Integrated systems and the no-tillage system exhibited a pore-size distribution with a higher proportion of micropores relative to macro- and mesopores, despite the sandy texture of the soil. In this context, soil organic carbon (SOC) plays a crucial role in the formation of intra-aggregate pores responsible for soil water retention, while also increasing the specific surface area available for water molecule adsorption. In summary, organic carbon acted as the main soil-structuring agent promoting the formation and stabilization of aggregates and generating a complex and efficient pore system that optimizes the balance between water retention (micropores) and air and water movement in the soil (meso- and macropores) [30]. Furthermore, soil organic carbon is positively associated with soil biological activity, with microporosity functioning as a structural component that provides protected bacterial habitats (pores ~0.3–0.5 μm) and is highly responsive to management practices [42]. In integrated systems, fine roots of the tree component may also contribute to increased subsoil microporosity in sandy soils, as root exudation of organic compounds is associated with greater carbon deposition and aggregation, which modify soil aggregates and affect microporosity and retained water content [22].

Across all systems, the most frequent pore radius (*Rmax*) was located within the macro- and mesopore ranges, except for the CLI system in the 0.0–0.10 m layer, where it occurred within the micropore range. *Rmax* represents the predominant soil pore size that drains most rapidly and is an important indicator of soil physical quality, reflecting soil structure and aeration capacity. The land-use history of the CLI system (soybean monoculture for 17 years), along with livestock integration during the early years of system adoption, may have increased surface soil compaction and reduced total porosity. Additionally, animal trampling on soil with low structural stability may have contributed to the transformation of well-connected structural pores (macropores and mesopores) into smaller, poorly connected pores (micropores).

Soil management strongly affects pore architecture, which is reflected in the pore-size distribution when evaluated using the soil water retention curve. Consequently,

management practices directly influence the most frequent pore radius (*Rmax*), shifting its occurrence among different classes of functional pore classes [31]. A study conducted in a physically vulnerable soil under conservation agriculture demonstrated a shift in the most frequent pore radius toward larger pore classes (macropores) compared with conventional management systems [31]. Moreover, management systems that enhance soil health, minimize disturbance, and increase soil organic carbon tend to redirect the most frequent pore radius toward domains controlled by biological activity [42]. In another study comparing rhizosphere and non-rhizosphere soils, the most frequent equivalent pore radius (*Rmax*) was observed within the mesopore class, with slightly higher values in rhizosphere soil (40.98 μm) than in non-rhizosphere soil (32.69 μm). This increase was attributed to enhanced aggregation induced by roots and higher soil organic carbon content [43].

4.3. Relative Soil Hydraulic Conductivity

Relative soil hydraulic conductivity in the evaluated systems reflected the organization of the soil pore network, as evidenced by the soil water retention curves and pore-size distribution. Native vegetation (NV) exhibited a more stabilized structural condition, which resulted in more balanced soil water movement, with water flow occurring preferentially through larger, well-connected pores and decreasing as soil water content declined. This dynamic is only possible because NV represents a system in equilibrium, characterized by continuous organic matter inputs, diverse root systems, active microbiota, and the absence of mechanical soil disturbance. Integrated agricultural systems and no-tillage management, depending on the duration of adoption, root system diversity, and organic matter inputs into the soil—such as in the NT and LFI systems—show improvements in soil water dynamics, particularly with respect to soil water permeability.

The CLI system, due to its land-use history and the short period of adoption of the integrated system, with smaller increases in total organic carbon contents, exhibited a pore network that limited water permeability, especially at the soil surface. This resulted in slow water movement, potentially leading to poor drainage. The CFI system also showed slower soil water movement in deeper layers, which is related to an increased proportion of micropores at those depths.

The relationship between soil management and relative soil hydraulic conductivity (*Kr*) is complex, as *Kr* is a function that represents the relationship between unsaturated and saturated soil hydraulic conductivity and indicates the rate at which soil drains from a saturated condition. In some cases, *Kr* may be less sensitive to management-induced soil changes than saturated hydraulic conductivity. In an investigation comparing aggregate properties of rhizosphere soil versus inter-row (bulk) soil, *Kr* curves as a function of effective relative saturation showed no significant differences between rhizosphere and non-rhizosphere soils [43].

Although management may not strongly modify *Kr*, integrated systems have been shown to increase saturated hydraulic conductivity through improvements in soil structure, which may be reflected in an overall enhancement of soil water conduction. In a study comparing saturated hydraulic conductivity in native Cerrado vegetation, an Integrated Crop–Livestock–Forest system, and pasture areas, higher values were observed under forest conditions; however, the integrated system was still considered a promising strategy for restoring hydrological cycles and ecological functions lost due to the conversion of Cerrado vegetation into pastures [4]. Moreover, when compared with monoculture systems or degraded pastures, Integrated Crop–Livestock–Forest systems (ICLF; Integração Lavoura-Pecuária-Floresta, ILPF) have demonstrated a positive and significant impact on saturated soil hydraulic conductivity [19].

Improvements in this property in Integrated Crop–Livestock–Forest systems are intrinsically linked to their capacity to restore soil pore structure and functionality [15,32]. The inclusion of trees (e.g., eucalyptus) leads to higher saturated hydraulic conductivity and infiltration rates compared with systems without trees. This effect is attributed to the formation of water channels and macropores created by living and decomposing tree roots; Integrated Crop–Livestock–Forest systems enhance pore connectivity and organization, which is reflected in greater water and air permeability. Trees in silvopastoral systems can also reduce surface runoff velocity, thereby favoring water infiltration and improving soil water storage capacity [15].

5. Conclusions

Integrated Crop–Livestock–Forest, Livestock–Forest, and Crop–Forest production systems, as well as the no-tillage system, enhanced soil water retention and availability, particularly in the subsurface layers.

Integrated systems featuring a forest component (Livestock–Forest and Crop-Livestock), through increased soil organic matter input, the presence of grasses, and crop rotation, promoted higher soil water retention, contributing to a more balanced physical environment regarding water storage and movement.

The no-tillage system—due to its longer adoption time, lack of soil disturbance, and surface protection—exhibited a more consolidated soil pore geometry, which resulted in higher water retention and availability for plants.

Overall, integrated production systems represent important strategies for productive sustainability in the MATOPIBA region of the Brazilian Cerrado by enhancing soil water retention and availability to plants, especially through the adoption of intercropping systems that incorporate forest components associated with grasses over long periods of time.

Author Contributions: Conceptualization and writing—original draft preparation, M.L.d.N.S.; conceptualization, project administration and writing—review and editing, L.F.C.L.; methodology and writing—review and editing, F.P.d.O. and F.F.B.; methodology, I.T.S., T.S.d.S., D.S.V. and R.C.d.S.M.; conceptualization, H.A.d.S., E.S. and J.O.L.O.J. All authors have read and agreed to the published version of the manuscript.

Funding: This research was funded by Fundação Agrisus (PA 3732/24).

Data Availability Statement: All data supporting the findings of this study are available from the corresponding author upon reasonable request.

Acknowledgments: The authors have reviewed and edited the output and take full responsibility for the content of this publication.

Conflicts of Interest: The authors declare no conflicts of interest. The funders had no role in the design of the study; in the collection, analyses, or interpretation of data; in the writing of the manuscript; or in the decision to publish the results.

References

1. Leite-Filho, A.T.; Soares-Filho, B.S.; Davis, J.L.; Abrahão, G.M.; Börner, J. Deforestation reduces rainfall and agricultural revenues in the Brazilian Amazon. *Nat. Commun.* **2021**, *12*, 2591. [CrossRef]
2. Anache, J.A.A.; Flanagan, D.C.; Srivastava, A.; Wendland, E.C. Land use and climate change impacts on runoff and soil erosion at the hillslope scale in the Brazilian Cerrado. *Sci. Total Environ.* **2018**, *622–623*, 140–151. [CrossRef]
3. Rodrigues, A.A.; Macedo, M.N.; Silvério, D.V.; Maracahipes, L.; Coe, M.T.; Brando, P.M.; Shimbo, J.Z.; Rajão, R.; Soares-Filho, B.; Bustamante, M.M.C. Cerrado deforestation threatens regional climate and water availability for agriculture and ecosystems. *Glob. Chang. Biol.* **2022**, *28*, 6807–6822. [CrossRef]

4. Glatzle, S.; de Almeida, R.G.; Barsotti, M.P.; Bungenstab, D.J.; Giese, M.; Macedo, M.C.M.; Stuerz, S.; Asch, F. Integrated Land-Use Systems Contribute to Restoring Water Cycles in the Brazilian Cerrado Biome. *Land* **2024**, *13*, 221. [CrossRef]
5. de Araújo, M.L.S.; Rufino, I.A.A.; Silva, F.B.; de Brito, H.C.; Santos, J.R.N. The Relationship between Climate, Agriculture and Land Cover in Matopiba, Brazil (1985–2020). *Sustainability* **2024**, *16*, 2670. [CrossRef]
6. Stone, L.F.; Carvalho, M.T.d.M.; da Silva, M.A.S.; Calil, F.N.; Siqueira, M.M.d.B.; Moura, T.M.; Trogello, E.; Machado, P.L.O.d.A.; Heinemann, A.B.; Rangel, A.d.C.M.; et al. Intrinsic soil properties shape water availability under changing land-use in contrasting soil textures. *Soil Adv.* **2025**, *4*, 100082. [CrossRef]
7. Tefera, M.L.; Carletti, A.; Altea, L.; Rizzu, M.; Migheli, Q.; Seddaiu, G. Land degradation and the upper hand of sustainable agricultural intensification in sub-Saharan Africa—A systematic review. *J. Agric. Rural. Dev. Trop. Subtrop. (JARTS)* **2024**, *125*, 63–83. [CrossRef]
8. Ahmed, F.; Shakeel, A.; Ahmad, S.; Kaur, N. Exploring the Linkages Between Land Degradation and Food Insecurity. *Asia.-Pac. J. Rural Dev.* **2025**, *35*, 71–90. [CrossRef]
9. Moura, T.M.; De Melo Carvalho, M.T.; Stone, L.F.; Madari, B.E.; de Castro Santos, D.; Alves, E.M.; Trogello, E.; Faustino, L.L.; de Almeida Machado, P.L.O. Newly implemented crop-livestock-forest systems increase available water and aeration in soils of the Brazilian Savannah. *J. Agric. Rural Dev. Trop. Subtrop.* **2023**, *124*, 149–158. [CrossRef]
10. Barbosa, L.R.; Souza, H.A.D.E.; Oliveira, F.P.D.E.; Nunes, L.A.P.L.; Leite, L.F.C. Physical-hydraulic properties of an ultisol under no-tillage and crop-livestock integration in the cerrado. *Rev. Caatinga* **2022**, *35*, 460–469. [CrossRef]
11. Liang, X.; Yu, S.; Ju, Y.; Wang, Y.; Yin, D. Integrated Management Practices Foster Soil Health, Productivity, and Agroecosystem Resilience. *Agronomy* **2025**, *15*, 1816. [CrossRef]
12. Mrunalini, K.; Behera, B.; Jayaraman, S.; Abhilash, P.C.; Dubey, P.K.; Swamy, G.N.; Prasad, J.V.N.S.; Rao, K.V.; Krishnan, P.; Pratibha, G.; et al. Nature-based solutions in soil restoration for improving agricultural productivity. *Land Degrad. Dev.* **2022**, *33*, 1269–1289. [CrossRef]
13. Chausson, A.; Turner, B.; Seddon, D.; Chabaneix, N.; Girardin, C.A.J.; Kapos, V.; Key, I.; Roe, D.; Smith, A.; Woroniecki, S.; et al. Mapping the effectiveness of nature-based solutions for climate change adaptation. *Glob. Chang. Biol.* **2020**, *26*, 6134–6155. [CrossRef]
14. Lal, R. Soil degradation as a reason for inadequate human nutrition. *Food Secur.* **2009**, *1*, 45–57. [CrossRef]
15. Ologunde, O.H.; Bello, S.K.; Busari, M.A. Integrated agricultural system: A dynamic concept for improving soil quality. *J. Saudi Soc. Agric. Sci.* **2024**, *23*, 352–360. [CrossRef]
16. De Moraes, A.; de Faccio Carvalho, P.C.; Lustosa, S.B.C.; Lang, C.R.; Deiss, L. Research on Integrated Crop-Livestock Systems in Brazil 1 A pesquisa em Sistemas Integrados de Produção Agropecuária no Brasil. *Rev. Ciênc. Agron.* **2014**, *45*, 1024–1031. [CrossRef]
17. Santos, C.C.D.; da Silva, T.S.; Cavalcante, M.; da Silva, R.G.; de Camargo, P.B.; Cherubin, M.R.; Cerri, C.E.P.; Maia, S.M.F. Changes in carbon stocks and quality of the soil organic matter under different arrangements of integrated livestock-forest systems in the semi-arid region of Brazil. *Soil Tillage Res.* **2026**, *256*, 106882. [CrossRef]
18. Matos, P.S.; Oliveira, J.d.M.; Carvalho, M.T.d.M.; Madari, B.E.; da Silveira, A.L.R.; Damian, J.M.; Moraes, P.A.d.O.; de Araujo, W.A.; Siqueira, M.M.d.B.; da Silva, R.R.; et al. Impact of land use intensification on key drivers of soil organic carbon pools in Brazil's Central-West. *CATENA* **2025**, *249*, 108636. [CrossRef]
19. Romanoski, V.S.; de Oliveira, L.B.; Figueiredo, G.C.; Mayer, M.A.; Cavalieri-Polizeli, K.M.V. Dynamic soil hydraulic properties in regenerative agriculture: Effects of crop and forest integration in livestock systems. *Soil Tillage Res.* **2025**, *253*, 106680. [CrossRef]
20. Vanolli, B.d.S.; Dias, H.B.; da Luz, F.B.; Lamparelli, R.A.C.; Magalhães, P.S.G.; Cherubin, M.R. Crop–Livestock Integrated Systems Improve Soil Health in Tropical Sandy Soils. *Agronomy* **2025**, *15*, 378. [CrossRef]
21. Carvalho, d.F.; César, P.; Pontes, L.d.S.; Barro, R.S.; Simões; Pinto, V.J.L.; Dominschek, R.; Cargnelutti, C.d.S.; Maurício; Martins, R.; et al. Integrated crop-livestock-forestry systems as a nature-based solution for sustainable agriculture. *Agrofor. Syst.* **2024**, *98*, 2309–2323. [CrossRef]
22. Matos, A.M.S.; Bonini, C.d.S.B.; Moreira, B.R.d.A.; Andreotti, M.; Heinrichs, R.; da Silva, D.T.; de Souza, J.A.L.; Santos, M.A.; Andrighetto, C.; Pavan, G.M.; et al. Long-Term Integrated Crop–Livestock–Forestry Systems Recover the Structural Quality of Ultisol Soil. *Agronomy* **2022**, *12*, 2961. [CrossRef]
23. Choudhary, S.; Rajpoot, S.K.; Tripathi, A.; Choudhary, M.; Radha, L.; Sen, M. Diversified Cropping Systems for Improving the Crop Productivity and Soil Health of Dryland Ecosystem. *Land Degrad. Dev.* **2026**, *37*, 419–437. [CrossRef]
24. Dusi, P. Role of Crop Diversification in Enhancing Soil Fertility and Agricultural Biodiversity in Mixed Farming Systems. *J. Environ. Sustain.* **2025**, *2*, 1–7.
25. Angelotti, F.; de Oliveira, A.R.; Signor, D.; Júnior, P.I.F.; Voltolini, T.V. Sustainable research initiatives focusing on agricultural adaptation to climate change in the Brazilian semiarid region. *Pesqui. Agropecu. Bras.* **2025**, *60*, e04136. [CrossRef]
26. Chakraborty, P.; Thotakuri, G.; Singh, N.; Dhaliwal, J.K.; Kumar, S. Crop-livestock integration influenced soil profile organic carbon and hydro-physical properties in converted grasslands to row crops. *Soil Tillage Res.* **2024**, *240*, 106093. [CrossRef]

27. Singh, N.; Kumar, S.; Jin, V.L.; Schneider, S. Short-term soil physical responses to grazing and cover crops in an integrated crop-livestock agroecosystem. *J. Soil Water Conserv.* **2022**, *77*, 516–527. [CrossRef]
28. Lima, J.D.P.; Torino, A.B.; da Silva, L.M.; Júnior, L.F.D.N.; de Brito, M.F.; Costa, K.A.d.P.; Silva, B.M.; Severiano, E.d.C. Crop-Livestock Integration Improves Physical Soil, Agronomic and Environmental Aspects in Soybean Cultivation. *Plants* **2023**, *12*, 3746. [CrossRef]
29. Ferreira, V.S.; de Oliveira, F.P.; da Silva, P.L.F.; Martins, A.F.; Pereira, W.E.; Santos, D.; de Souza, T.A.F.; dos Santos, R.V.; Campos, M.C.C. Physical-Hydric Properties of a Planosols Under Long-Term Integrated Crop–Livestock–Forest System in the Brazilian Semiarid. *Forests* **2025**, *16*, 1261. [CrossRef]
30. Lal, R. Soil organic matter and water retention. *Agron. J.* **2020**, *112*, 3265–3277. [CrossRef]
31. Sandram, I.; Namaona, W.; Magwero, N.; Mbanyele, V.; Miti, C.; Moombe, M.; Mtangadura, T.; Lubinga, P.; Chisanga, C.; Nyagumbo, I.; et al. Fitting and comparing water retention curves for soils under contrasting experimental treatment: Examples from conservation agriculture trials in southern Africa. *Geoderma* **2025**, *461*, 117431. [CrossRef]
32. Fu, Z.; Hu, W.; Beare, M.; Thomas, S.; Carrick, S.; Dando, J.; Langer, S.; Müller, K.; Baird, D.; Lilburne, L. Land use effects on soil hydraulic properties and the contribution of soil organic carbon. *J. Hydrol.* **2021**, *602*, 126741. [CrossRef]
33. Hussain, A.; Bashir, H.; Zafar, S.; Rehman, R.; Khalid, M.; Awais, M.; Sadiq, M.; Amjad, I. The importance of soil organic matter (som) on soil productivity and plant growth. *Biol. Agric. Sci. Res. J.* **2023**, *2023*, 11. [CrossRef]
34. dos Santos, H.G. *Sistema Brasileiro de Classificação de Solos*, 5th ed.; Embrapa: Brasília, Brazil, 2018; Volume 1.
35. Staff, S.S. *Keys to Soil Taxonomy*, 13th ed.; USDA Natural Resources Conservation Service: Washington, DC, USA, 2022; Volume 1.
36. van Genuchten, M.T. A Closed-form Equation for Predicting the Hydraulic Conductivity of Unsaturated Soils. *Soil Sci. Soc. Am. J.* **1980**, *44*, 892–898. [CrossRef]
37. Libardi, P.L. *Dinâmica da Água no Solo*, 3rd ed.; Edusp: São Paulo, Brazil, 2018; Volume 1.
38. Koorevaar, P.; Menelik, G.; Dirksen, C. *Elements of Soil Physics*, 1st ed.; Elsevier: Amsterdam, The Netherlands, 1983; Volume 13.
39. Silva, M.L.D.N.; Libardi, P.L.; Gimenes, F.H.S. Soil Water Retention Curve as Affected by Sample Height. *Rev. Bras. Cienc. Solo* **2018**, *42*, 0180058. [CrossRef]
40. Mualem, Y. A new model for predicting the hydraulic conductivity of unsaturated porous media. *Water Resour. Res.* **1976**, *12*, 513–522. [CrossRef]
41. Tian, M.; Qin, S.; Whalley, W.R.; Zhou, H.; Ren, T.; Gao, W. Changes of soil structure under different tillage management assessed by bulk density, penetrometer resistance, water retention curve, least limiting water range and X-ray computed tomography. *Soil Tillage Res.* **2022**, *221*, 105420. [CrossRef]
42. Bodner, G.; Zeiser, A.; Keiblinger, K.; Rosinger, C.; Winkler, S.K.; Stumpp, C.; Weninger, T. Managing the pore system: Regenerating the functional pore spaces of natural soils by soil-health oriented farming systems. *Soil Tillage Res.* **2023**, *234*, 105862. [CrossRef]
43. Batista, A.M.; Pessoa, T.N.; Putti, F.F.; Andreote, F.D.; Libardi, P.L. Root Influences Rhizosphere Hydraulic Properties through Soil Organic Carbon and Microbial Activity. *Plants* **2024**, *13*, 1981. [CrossRef]